Low sulphated heparins target multiple proteins for central nervous system repair

McCanney GA[1], McGrath MA[1], Otto TD[1], Burchmore R[1], Yates EA[3], Bavington C[2], Willison HJ[1] , Turnbull JE[3], Barnett SC[1]

[1]Institute of Infection, Immunity and Inflammation, College of Medical, Veterinary and Life Sciences, University of Glasgow, 120 University Place, Glasgow G12 8TA, UK

[2]GlycoMar Limited, European Centre for Marine Biotechnology, Dunstaffnage Marine Laboratory, Dunbeg, Oban Argyll, Scotland, PA37 1QA.

[3]Department of Biochemistry, Institute of Integrative Biology, University of Liverpool, Liverpool, United Kingdom

McGrath MA, and McCanney GA are joint first authors.

Running title: Heparin mimetics as CNS therapeutics

*corresponding author:
Professor Sue Barnett
University of Glasgow, Institute of Infection, Immunity and Inflammation, College of Medical, Veterinary and Life Sciences, GBRC, Room B329,
120 University Place, Glasgow, G12 8TA.
Telephone: 44 (0)141 330 8409 E-mail: Susan.Barnett@Glasgow.ac.uk

Total number of words: 12,752, Number of pages: 31, Number of figures: 8, Tables: 1,
Number of words for Abstract: 246, Materials and Methods: 2813, Introduction: 649, and Results: 2464, Discussion: 2000, References: 2218, Legends: 1607.

Key words: heparan sulphates, myelination, neurite outgrowth, amyloid-β
Conflict of interest: The authors declare no competing financial interests
Acknowledgments: The work was supported by a project grant ETM/439 from CSO (MM) and a PhD studentship (PhD-769-2014) from Medical Research Scotland (GM), and the Wellcome Trust (202789/Z/16/Z). We also thank bioinformaticians at Glasgow Polyomics for their advice and help on the mass spectrometry,

ABSTRACT

The lack of endogenous repair following spinal cord injury (SCI) accounts for the frequent permanent deficits for which effective treatments are absent. Previously, we demonstrated that low sulphated modified heparin mimetics (LS-mHeps) attenuate astrocytosis, suggesting they may represent a novel therapeutic approach. mHeps are glycomolecules with structural similarities to resident heparan sulphates (HS), which modulate cell signaling by both sequestering ligands, and acting as cofactors in the formation of ligand-receptor complexes. To explore whether mHeps can affect the myelination and neurite outgrowth necessary for repair after SCI, we created lesioned or demyelinated neural cell co-cultures and exposed them with a panel of mHeps with varying degrees and positions of their sulphate moieties. LS-mHep7 enhanced neurite outgrowth and myelination, whereas highly sulphated mHeps (HS-mHeps) had attenuating effects. LS-mHeps had no effects on myelination or neurite extension in developing, uninjured myelinating cultures, suggesting they might exert their proregenerating effects by modulating or sequestering inhibitory factors secreted after injury. To investigate this we examined conditioned media from cultures using chemokine arrays, and conducted an unbiased proteomics approach by applying TMT-LC/MS to mHep7 affinity purified conditioned media from these cultures. Multiple protein factors reported to play a role in damage or repair mechanisms were identified, including amyloid betaA4. Amyloid beta peptide (1-42) was validated as an important candidate by treating myelination cultures and shown to inhibit myelination. Thus, we propose that LS-mHeps exert multiple beneficial effects on mechanisms supporting enhanced repair, and represent novel candidates as therapeutics for CNS damage.

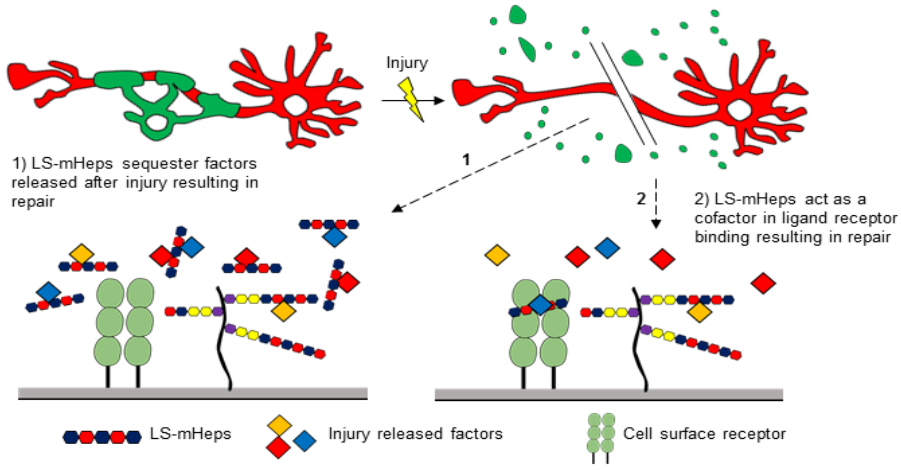

Main Points

- After CNS injury a host of heparin binding-factors are secreted which affect repair.
- Low sulphated modified heparin mimetics (LS-mHeps) bind to multiple factors exerting beneficial effects on CNS repair.
- Using TMT/LC-MS we identified amyloid betaA4 as a demyelination factor**.**

INTRODUCTION

Spinal cord injury (SCI) is predominantly caused by mechanical and ischemic trauma to the spinal cord. As the CNS has limited regenerative and repair capacity, any function loss is generally permanent. The pathophysiology of SCI comprises both a primary and secondary cascade of injury mechanisms (Dumont et al., 2001). The former causes axonal transection, cellular damage and disruption of the blood brain barrier (BBB) while the latter leads to local neuronal cell death and Wallerian degeneration, accompanied by the initiation of an intense immune response. The CNS responds to these events by forming a glial scar rich in reactive astrocytes, myelin-associated inhibitors, microglia, macrophages, and meningeal fibroblasts which play a major role in sequestering damaged tissue in a relatively impermeant environment (Filous and Silver, 2016). Thus, any repair strategies for SCI must consider multifactorial pathways including disruption of the scar, promotion of axonal outgrowth and remyelination.

Previously, we used a confrontation assay to study the effects of astrocytosis, characterising boundary formation, expression of GFAP and astrocyte hypertrophy (Lakatos et al., 2000; Wilby et al., 2000). We found that Schwann cells do not mingle with astrocytes whereas olfactory ensheathing cells (OECs) mingle well (Lakatos et al., 2000). We identified heparin and FGFs as strong inducers of boundary formation between astrocytes and OECs and concluded that highly sulphated heparan sulphates (HS) secreted by Schwann cells induced the astrocyte-Schwann cell boundary (Fairless et al., 2005; Santos-Silva et al., 2007)

HS are linear sulphated polysaccharides that play an important role in regulating many mammalian cellular processes. They exist as proteoglycans (HSPG) in which two or three HS chains are attached to core proteins at the cell surface, or as extracellular matrix (ECM) proteins. It is thought that the pattern, epimerization and degree of sulphation is important in facilitating HS-ligand interactions, thereby enabling HS to function as a key regulator of complex cell signaling mechanisms in development, regulation of chemokine function, angiogenesis and blood coagulation, in both normal and disease states (Bishop et al., 2007; Cui et al., 2013, Changyaleket et al., 2017). To investigate how HS sulphation characteristics influence astrocytosis we applied a panel of modified heparins (mHeps) which have been selectively desulphated in the confrontation assay. We found that mHeps with low sulphated (LS-) moieties could attenuate the astrocytic behavior, whereas highly sulphated (HS-) mHeps induced a strong reactive astrocyte response in culture (Higginson et al., 2012). This led us to hypothesize that modifying the level of HS

sulphation in the vicinity of astrocytes might be a therapeutic approach to promoting one pathway involved in CNS repair (O'Neill et al., 2017).

Whilst the above addresses effects on astrocytosis, if mHeps are to be developed for treatment of the injured CNS, there is a need to investigate possible effects on other neural cells. We therefore studied the effect of mHeps on myelinating cultures generated from dissociated spinal cord cells. These basic cultures are referred to as myelinating cultures–development (MC-Dev). Secondly, an adaptation of MC-Dev can be used to model aspects of CNS injury by cutting mature cultures with a scalpel blade, generating a cell-free area characterized by a persistent lack of neurite outgrowth. Over time, the cell free area becomes infiltrated with reactive astrocytes, and microglia, as seen in animal models of CNS injury. These cultures are termed MC-Inj (Boomkamp et al., 2012). Finally, mature myelinating cultures can be used to investigate demyelination by treating them with anti-MOG antibody plus complement which resulted in demyelination of axons (Elliot et al., 2012; MC-Demy). When the panel of differentially sulphated mHeps were applied to these 3 cultures types, we found that LS-mHeps not only attenuate astrocytosis, but also exert positive effects on neurite outgrowth and remyelination suggesting these glycomolecules may be an important novel therapeutic for CNS damage. Using TMT-LC/MS and chemokine array of secreted factors from the two injury culture models we identified differences in heparin binding proteins suggesting subtle difference in mechanisms.

MATERIALS AND METHODS

Astrocytes Derived From Neurospheres

Neurospheres (NS) were generated from the striata of 1-day-old Sprague Dawley (SD) rat using a method modified by (Reynolds and Weiss 1996) and differentiated into astrocytes as described in (Sorensen et al. 2008). Briefly, the tissue was enzymatically dissociated and plated in neurosphere medium (NSM) containing, Dulbecco's Modified Eagle Medium/F12 (DMEM/F12, 1:1, DMEM containing 4,500 mg/L glucose), enriched with 0.105% $NaHCO_3$, L-glutamine, 5,000 IU/mL penicillin, 5 µg/mL streptomycin, 5.0 mM HEPES (all from Invitrogen, UK), 100 µg/mL apotransferrin, 25 µg/mL insulin, 60 µM putrescine, 20 µM progesterone, and 30 µM sodium selenite, supplemented with 20 ng/ml of epithelial growth factor (EGF) (Peprotech, UK). The cell suspension was maintained until neurospheres were formed. To generate astrocytes the neurospheres were triturated to produce smaller cell sphere suspensions, transferred to 13 mm poly-$_L$-lysine (PLL), 13µg/ml, Sigma) coated coverslips in a 24-well plate (Corning, UK) and incubated for a further 5-7 days *in vitro* (DIV) at 37ºC in an atmosphere of 7% CO_2/93% air until

a confluent monolayer formed. Neurosphere-derived astrocytes were maintained in DMEM (1 g/ml glucose) with 10% foetal bovine serum (Sigma) and 2 mM L-glutamine (Sigma)

Modified heparins.

Selectively chemically desulphated mHeps were prepared as described previously (Higginson, et al., 2012). The compounds described here had predominant repeating structures as follows (LS, low sulphated; HS, high sulphated): HS-mHep 1, IdoA(2S)-GlcNS(6S); LS-mHep6, IdoA(2S)-GlcNAc; LS-mHep7, IdoA-GlcNS; LS-mHep8, IdoA-GlcNAc.

Myelinating spinal cord cultures (MC-Dev and MC-Inj)

Generation of rat spinal cord mixed cell cultures (myelinating cultures, MC) was based on our previously described methods (Sorensen et al. 2008; Boomkamp et al., 2012, 2014). The spinal cord of E15.5 SD embryos were enzymatically dissociated and the resulting cell suspension at 300,000 cells per 50 µl, were plated on top of the neurospheres derived astrocytes on coverslips in plating medium (PM) that contained 50% Dulbecco's modified Eagle's medium (DMEM-1 g/ml glucose), 25% horse serum, 25% HBSS with Ca^{2+} and Mg^{2+}, and 2 mM L-glutamine. Cells were left to adhere for 2 hr at 37°C, then supplemented with 300 µl PM and 500 µl differentiation medium which contained DMEM (4.5 g/ml glucose), 10 ng/mL biotin, 0.5% hormone mixture (1 mg/mL apotransferrin, 20 mM putrescine, 4 lM progesterone, 6 lM selenium (formulation based on N2 mix of (Bottenstein and Sato, 1979) 50 nM hydrocortisone, and 0.5 mg/ml insulin known as DM+, or DM- if lacking insulin (all reagents from Sigma). Each 35 mm Petri dish containing 3 myelinating culture coverslips was fed three times a week by removing 400µl of medium and adding 500 µl fresh DM+ for 12 DIV then DM- for the proceeding 12 DIV. Cultures were maintained for 24-35 DIV in an atmosphere of 7% $CO^{2/}$93% air at 37 ^{o}C and referred to as MC-Dev. Over time these cultures elaborate myelinated fibres interspaced with organised nodes of Ranvier (Sorensen et al., 2008), with normal periodicity and compaction (Thomson et al., 2008). To assess the effect of mHeps on developmental myelination, cultures were treated at 13 DIV and 20 DIV (1 ng/ml). Furthermore, MC-Dev cultures underwent a single treatment at 24 DIV to assess if mHeps (1 ng/ml) had an effects on mature myelin. Following which both sets of cultures were fixed and stained at 28 DIV. MC-Dev cultures were treated with amyloid beta (Aß)-peptide (1-42) rat (TOCRIS-2425) at 16, 19 and 21 DIV (1 µM) or combined with 100 $ngmL^{-1}$ mHep7 during feeding. The cultures were fixed and stained at 18, 20, 22 and 24 DIV for myelin quantification (described below). Additionally, conditioned media was collected for CytoTox 96® Non-Radioactive Cytotoxicity Assay (Promega G1780).

For generating MC-Inj, at 24 DIV myelinating cultures were cut using a 11 mm single edge razor blade (WPI, Aston, UK) pressed gently across the center of the coverslip. Details can be found in Boomkamp et al., 2012, 2014. The cut created a rapid focal cell free area (650 μm) with a decrease in neurite density and myelination levels adjacent to it and very low numbers of neurites crossing the cut area site, referred to as the lesion. Using these cultures lesion size, neurite density and outgrowth and myelination can be assessed using immunocytochemistry, PCR and Western blotting.

MC-Inj respond appropriately to treatment with compounds reported to be effective in animal models of CNS injury, corroborating MC-Inj as a moderate throughput screen for CNS injury (Boomkamp et al., 2012, 2014). The cultures were treated with each mHep at a concentration of 1 ng/ml for a single treatment after 25 DIV and allowed to recover for a further 5 DIV, cultures were then fixed and stained as described below.

Demyelinated cultures (MC-Demy)

To assess remyelination the myelinating cultures were set up and maintained as described above. At 24 DIV, when many fibres are myelinated, the cultures were demyelinated by overnight incubation with the Z2 antibody (100 ng/ml Hybridoma, kind gift from Prof C Linington) which recognises myelin oligodendrocyte glycoprotein (MOG) and rabbit complement (100 μg/ml, Millipore) at 37°C. The Demyelinated cultures were then washed with DM- to remove excess complement and treated with the panel of mHeps at 1 ng/ml. At 30 DIV the cultures were fixed and stained as described below.

Conditioned medium (CM) collection

To obtain medium conditioned by the various cultures, MC-Inj and MC-Demy were set up. Conditioned media was collected after 25 DIV, for the cut conditioned medium (CCM) and demyelination conditioned media (DCM) this was 24 hours after cultures had been cut and demyelinated respectively. Uninjured culture conditioned medium (UCM) was also collected from myelinating cultures at 25 DIV as control. CM was also taken after treatment at 26 and 28 DIV (corresponding to days 1 and 3 post treatment). The CMs were added to MC-Dev at 16, 19 and 21 DIV. CM was diluted 1:4 with DM- or combined with 1 ng/ml mHep 6. At 24 DIV the cultures were fixed and stained as described below.

Cytokine array screen

Conditioned medium from each type of MC was collected as described above and 1.5 ml was assayed in a Proteome Profiler Rat XL Cytokine Array (R&D Systems, ARY030) using the manufacturer's protocol. The array simultaneously detects levels of 79 rat cytokines, chemokines, growth factors and other soluble proteins (see https://www.rndsystems.com/products/proteome-profiler-rat-xl-cytokine-array_ary0300. Comparisons of CCM and DCM was made to UCM, using semi-quantitative densitometry analysis on Total Lab Quant Software (TotaLab Limited). Using the circle tool each dot was individually quantified with duplicates averaged and the integrated density values compared.

Oligodendrocyte progenitor cell culture

Oligodendrocyte progenitor cells (OPC) were isolated from cortical astrocyte monolayers generated from postnatal day 1 (P1) SD pups as previously described (Noble and Murray, 1984). Once a confluence astrocyte monolayer formed the OPCs were detached by controlled agitation of the flask, and quickly plated onto a 90 mm culture dishes for 15-20 min. OPCs were separated from other glia cells by differential adhesion (Miron et al., 2013**)**. OPCs remained in the supernatant, which was removed, centrifuged and the OPCs resuspended in serum-free DMEM-BS (adapted from Bottenstein and Sato, 1979) containing 0.5 mg/ml insulin in 10 mM HCL (Sigma, UK), glutamine (100 mM; Sigma, UK, human transferrin (Sigma, UK) and gentamycin (100 mg/ml; Sigma, UK), supplemented with the growth factors; fibroblast growth factor (FGF-2) at 10 ng/ml and platelet derived growth factor (PDGF) at 2 ng/ml (both Peprotech, UK). The isolated OPCs were plated on poly-L-lysine (PLL, Sigma, 13µg/ml) coated glass coverslips (VWR) in a 24-well plates at a density of 5,000 cells in 50 µl drop and allowed to attach. They were maintained in DMEM-BS containing PDGFα and FGF2 for 5 days and then switched to DMEM-BS lacking growth factors and with or without mHeps at a concentration of 1 ng/ml. Cultures were used for proliferation, morphology and differentiation assays.

Nanofibres

OPCs were seeded onto PLL coated nanofiber culture inserts (Nanofiber Solutions TM) at a density of 25,000 cells in DMEM-BS containing PDGFα and FGF2 and incubated for 5 DIV. The OPC medium was then switched to DMEM-BS containing mHeps at 1 ng/ml for 7 DIV. Purified OPCs sheath length was quantified after mHep treatment by measuring a single internode (PLP+ process) per cell, from cell body to outmost internode and cell size by measure the surface area of each cell in ImageJ.

Immunohistochemistry

MC were fixed with 4% PFA for 20 min at room temperature (RT) and permeabilised with 0.2% Triton X-100 at RT for 15 min, blocked with PBS with 0.2% porcine gelatin prior to addition of primary antibodies for 1 hr at RT. For extracellular labelling, the cultures were incubated with primary antibodies for 20 min at RT. Oligodendrocyte lineage cells were visualised with the O4 antibody (1:1, mouse IgM hybridoma: Sommer and Schachner, 1981). Cells were washed, incubated with the appropriate secondary Alexa fluorophore-conjugated antibody for 20 min at RT and fixed in ice-cold methanol for 15 min at -4ºC. For co-labelling with intracellular antibodies, cells were incubated with primary antibodies, diluted in blocking buffer (containing PBS with 0.1% Triton X-100 and 0.2% porcine gelatin) for 45 min at RT followed by the appropriate secondary Alexa fluorophore-conjugated antibodies for 45 min at RT. The cells were washed and mounted in Vectashield (Vector Laboratories, Peterborough, UK).

For intracellular labelling alone, the cultures were fixed in 4% paraformaldehyde for 20 min at RT followed by washes in PBS and permeabilization in 0.2% Triton- X100 for 15 min at RT. The primary antibodies were added, diluted in blocking buffer, and the cells incubated for 45 min at RT. Mature myelin (PLP) was visualised using AA3 antibody (1:100, anti-rat; hybridoma supernatant, Yamamura et. al. 1991), Neurofilament was detected using SMI31 (mouse IgG1, 1:1500, BioLegend). After washing, the cultures were incubated with the appropriate secondary antibodies at RT for 45 min. The cells were washed in PBS followed by dH_2O, mounted in Vectashield (Vector Laboratories, Peterborough, UK).

EdU Cell Proliferation assay

For proliferation studies OPCs were isolated as described above, but maintained for only 2 days in DMEM-BS containing PDGFα and FGF2. The cells were then switched into DMEM-BS lacking growth factors for 24 hours (except for the PDGF/FGF condition) before treatment with mHeps, along with immediate incubation with 10 mM of 5-ethynyl-2′-deoxyuridine (EdU) for 18 hr. EdU detection was performed using Click-iT EdU imaging kit (C10084, Invitrogen) per manufacturer's instructions. The OPCs were then immunolabelled with Olig2 (Rabbit polyclonal, 1:500, Millipore,UK) following which cultures were washed and mounted as previously described.

Microscopy and Image analysis

Cells were imaged using Olympus BX51 or LAS AF Leica DM4000 B fluorescence microscopes, a Zeiss LSM 510 confocal microscope. For quantitative analysis of injury; neurite density,

myelination and neurite outgrowth, the entire lesion site was imaged adjacent (0–670 μm from the lesion edge) and the actual injury site with each condition being blinded to the experimenter. Similarly, for the MC-Dev and MC-Demy quantification of neurite density and myelination each condition was blinded to the experimenter and standardised random sampling was performed. For neurite density, myelination and neurite outgrowth studies images were taken at 10x magnification with 20 images per coverslip. Cell counting analysis was made for OPCs and OLs respectively at 10x and 20x magnifications with 10 images per coverslip. The cells of interest were counted per field of view and divided by the total number of DAPI-positive cells.

Myelination and OPC/OL quantification

Quantification was carried out using CellProfiler Image Analysis software (Broad Institute) (Carpenter, 2006; Lindner et al., 2015). For neurite density, the threshold level pixel value for SMI31 immunoreactivity (IR) was divided by the total number of pixels. The percentage of myelinated axons, (PLP) was measured using CellProfiler, which uses pattern recognition software to distinguish between linear myelinated internodes and oligodendrocyte cell bodies. In this manner we track the co-expression of myelin sheaths (PLP) and axons (SMI31), and calculate this percentage of myelinated fibres. All experiments were carried out at least three times in duplicate. For OL quantification images adjacent to the lesion were used and OL cells were calculated using a Cellprofiler pipeline which counts the presence of PLP+ cell bodies overlapping DAPI nuclei. OPC/OL cultured on nanofibers were analysed for cell size and myelin internode length. Both were calculated using ImageJ software. Two measurements per cell were taken measure from the cell body to the outmost myelin internode 20 cells were used per image selected at random. The cell size was defined by the green (PLP+) pixel threshold compared to the total pixel intensity and individual cells were marked with region of interest (ROI) tool to allow single cell analysis. All cellProfiler pipelines used in this study are available at https://github.com/muecs/cp.

Neurite outgrowth and lesion size quantification

10 Images of the cut in the MC-Inj were collected using random sampling. Neurite outgrowth was defined as a SMI31 positive projection which enters and crosses the lesion site. In each image the number of neurites which cross the lesion site were counted. Any area around the lesion that appeared uninjured was excluded from analysis. The number of neurites per images was averaged across the lesion and termed neurite outgrowth per field of view. Using the same images, the width of the lesion was calculated using ImageJ at 10 fields of view per lesion, averaged and termed lesion width (μm).

Heparin binding proteins (HBPs) pull down and mass spectroscopy (MS) analysis

CCM, DCM and UCM were affinity purified on an mHep7 column. To make the column a commercial HiTrap NHS-activated HP column (1 mL, GE Healthcare) was washed extensively with ddH2O (20 mL) and 10 mg (1 mL) of mHep7 was introduced onto the column and allowed to react at 15^0C for 2 h. Any unbound mHep7 was washed off the column with ddH2O (20 mL) and a small soluble amine (5% ethanolamine in ddH2O) was added to react with any remaining N-hydroxysuccinimide (NHS) groups at 15^0C for 2 h. The column was washed with PBS (pH 7.5, 20 mL) and ready for use to capture mHep7 binding proteins. Six ml of the different CM was run down the column with a peristaltic pump, following the manufacturer's instructions. Binding buffer and elution buffer was 10 mM sodium phosphate, pH7 and 10mM sodium phosphate, 1M NaCl pH 7 respectively. The eluted heparin binding proteins were desalted and concentrated using Amicon Ultra-15 centrifugal device (3K, 15mL. Millipore, UK). The proteins were digested with trypsin, using the FASP protocol (Wisniewski, 2009) and analysed by LC-MS using an Orbitrap Elite MS (Thermo Scientific) as described previously (Akpunarlieva, 2017). Protein identifications were assigned using the Matrix Science MascotDaemon server (Mascot) search engine to interrogate protein sequences in the Uniprot database RAT genome, allowing a mass tolerance of 10 ppm for the precursor and 0.6 Da for MS/MS matching.

To obtain quantitative data UCM, CCM and DCM were also analysed by tandem mass tag (TMT) labelling and liquid chromatography–mass spectrometry (LC-MS). The samples were digested with trypsin to generate peptides that were differentially labelled with multiplex tandem mass tags as previously described (Bilic, 2018). Samples were then mixed and analysed by LC-MS. The TMT plates are 6-plex to enable multiplex analysis and the resulting peptides, covalently labelled with TMT tags, were solubilized in 2 % acetonitrile with 0.1 % trifluroacetic acid and fractionated on a nanoflow uHPLC system (Thermo RSLCnano) before online analysis by electrospray ionisation (ESI) mass spectrometry on an Orbitrap Elite mass spectrometer. Peptide separation was performed on a Pepmap C18 reversed phase column (LC Packings). The output from the LC-MS/MS was deconvoluted using ProteomeDiscoverer software, with advice from bioinformaticians at Glasgow Polyomics, and the relative change in abundance of proteins between samples for comparison was determined, with statistical significance assessed by analysis of variance between replicates using Minitab. Any value with a Mascot score of greater than 70 was considered significant and those with Mascot scores below 20 were discounted**.**

Amyloid beta (Aβ) (1-42) and (1-40) ELISAs

MC-Demy cultures were treated with mHep7 (1 ng/mL) and media collected at 26 and 28 DIV (equating to days 1 and 3 post treatment respectively). This CM and mHep7 eluate described above were tested using an amyloid beta petide 1-42 and 1-40 ELISAs (Thermofisher, KHB3441/KHB3481) as per manufacturer's description.

Statistical analysis

Graphpad Prism software was used for data presentation and statistical testing. For simple comparison paired-students t-test was employed to determine statistical significance. For multiple condition comparisons One-way repeated measures ANOVA test was employed to data sets followed by Dunnett's multi-comparison test or Holm-Sidak post-hoc correction to calculate potential significant difference. Asterisks are used to represent significance less than *$p<0.05$, **$p<0.01$, ***$p<0.001$ and inserted onto graphed data. All errors are depicted as standard errors of the mean (SEM). A minimum of 3 technical repeats/experiment and at least 3 biological (n) repeats were made. Gene Ontology term enrichment analysis was performed in R, using TopGO (Alexa et al., 2016). As a Gene Ontology database we used the GO term from Uniprot. To correct for multi testing, we multiply the P-value by the amount of statistical test that were performed.

RESULTS

Selectively desulphated mHeps promote neurite outgrowth and myelination in myelinating culture-injured (MC-Inj).

The effects of a number of selectively desulphated mHeps (Higginson, et al., 2012; O'Neill et al., 2017) on neurite density, myelination, neurite outgrowth and lesion size following injury, were assessed using the MC-Inj model. Fig. 1A-E are representative images of levels of myelination adjacent to the lesion in cut control (A) and mHep (B-E) treated MC-Inj. It can be seen that the percentage of myelinated fibres was significantly higher after treatment with the low- or de-sulphated mHeps6-8 increasing to 8-10% from 5% in untreated control ($p = 0.0017$, < 0.0001 and 0.0001 for mHep6, 7 and 8 respectively), but treatment with HS-mHep 1 resulted in a decreasing trend to 2.5% although this appears non-significant (Fig. 1C-E, quantification in panel F). Neurite density was analysed adjacent to the injury site and a significant increase ($p = 0.0127$) was observed after treatment with LS-mHep6 compared to the untreated control, whereas the other mHeps1, 7 and 8 had no significant effect on neurite density (Fig. 1G). Fig. 1H-L show representative images of neurites crossing the lesion and the lesion size in control and treated cultures. . Quantification of the average number of neurites in the lesion is shown in Fig. 1M. The LS-mHeps 6-8, all significantly promoted neurite outgrowth across the lesion compared to the

untreated control ($p = 0.0172$, < 0.0001 and 0.0029 for mHep6, 7 and 8 respectively). The HS-mHep1 did not promote neurite outgrowth after treatment, with neurite numbers being similar to the untreated control (~3 neurites/field of view). Lastly, the width of the lesion was quantified after mHep treatment (Fig. 1N). HS-mHep1 treatment resulted in a significant increase in lesion size (564 ± 27.5 μm, $p = 0.0026$) compared to the untreated control (400 ± 20.0 μm, Fig. 1H, I and N). In contrast the LS-mHeps6-8, did not significantly affect the lesion size, with average lesion sizes being, 315.2 ± 46.8 μm (mHep6), 405 ± 48.6 μm (mHep7) and 317 ± 56.2 μm (mHep8).

LS-mHeps promote oligodendrocyte process extension.

To determine the effect of the mHeps directly on OPCs we treated purified OPCs with 1 ng/ml of mHeps. Firstly we established that OPC proliferation was unaffected by any mHep treatment when compared to DMEM-BS control, and PDGF/FGF2 treatment, a growth factor cocktail known to promote OPC proliferation ($p = 0.0032$; Fig. 2A-C). Representative images of the control and PDGF/FGF treated OPCs are shown in Fig. 2A and 2B respectively. HS-mHep1 treatment induced a significant decrease in OL numbers adjacent to the lesion compared to the untreated control (Fig. 2F, $p = 0.0336$). Conversely, LS-mHep6 and 7 treatment resulted in a significant increase in the number of OLs adjacent to the lesion site compared to control (Fig. 2F, $p = 0.0133$ and 0.0002).

To investigate whether mHeps directly affect OPC process wrapping we used nanofibers which allow the study of ensheathment in the absence of dynamic neuronal signaling (Lee et al., 2012). The OL sheath length in DMEM-BS alone (control) averaged 166.6 ± 20.4 μm with the growth factor control (PDGF/FGF) cell size only reaching 87.3 ± 31.2 μm (Fig. 2G,L). HS-mHep1 had no significant effect on the sheath length with the average length reaching 150.6 ± 57.9 μm (Fig. 2H, L). Similarly, the LS-mHep7, had no significant effect on the sheath length with average lengths measuring 196.9 ± 60.2 μm (Fig. 2J, L). The cell area of OLs was significantly increased following treatment with LS-mHep7 (289.2 ± 49.8 μm^2, $p < 0.0001$) compared to control (139 ± 16.9 μm^2; Fig 2J-K). Treatment with LS-mHep6 and 8 did not affect cell area (157.9 ± 41.9 and 141.9 ± 36.9 μm^2, respectively), however, HS-mHep1 treatment caused a non-significant decrease in the overall cell area, (79.7 ± 8.3 μm^2; Fig. 2H), Moreover, LS-mHep6 and 8 treatment induced a significant increase in the OL sheath length compared to control with an average length of 298.6 ± 84.3 μm and 317.4 ± 66.7 μm respectively (Fig. 2I,K, $p = 0.0001$ for both).

mHep treatments have no effect on myelination levels in MC-Dev.

Rat myelinating cultures (MC-Dev) were treated with mHeps1,6 and 7 (1 ng/ml) after 13 DIV or 24 DIV, fixed and stained at 28 DIV and the percentage of myelination and neurite density within the cultures quantified. Fig. 3A-D illustrates representative images of control and treated cultures after mHeps were added from 13 DIV while Fig 3G-J show their effects when added from 24 DIV. Myelination and neurite density were quantified and shown in Fig. 3E,K and F,L respectively. It can be seen that mHep treatments did not significantly affect either myelination levels or neurite density in MC-Dev when added from 13 DIV compared to untreated control. In contrast when treatment occurred at 24 DIV, once more fibres were myelinated, and it was seen that the addition of mHep1 and mHep7 resulted in a significant decrease in myelination when compared to untreated controls (Fig 3K, $p = 0.0033$ and 0.0163 respectively), although neurite density was not affected (Fig 3L).

LS-mHep treatment enhances CNS remyelination

Since the developmental myelination in MC-Dev was essentially unaffected by treatment with mHeps we hypothesized that the injury environment produced by MC-Inj may be essential to their effectiveness in promoting myelination. We propose that similar effects would be seen in a different CNS injury environment. To address this we used MC-Demy, in which MC-Dev cultures were demyelinated with complement and anti-MOG antibody followed by a single treatment with mHeps (1 ng/ml), and maintained until 30 DIV, followed by staining for PLP and SMI31 to visualize myelination and neurites respectively. Fig. 4A-F shows representative images and Fig 4, G,H the quantification of myelination and neurite density respectively. It can be seen that LS-mHeps treatment increased the percentage of myelinated fibres by 70-80% compared to the demyelinated control (Demy5) without affecting neurite density ($p = 0.0002$, 0.0004 and 0.0002 for mHep6, 7 and 8 respectively). This suggests that the LS-mHeps enhance remyelination in this injury environment, absent of any toxic effects on neural cells.

Conditioned medium collected from MC-Inj (CCM) reduces CNS myelination

Since we only observed effects on myelination using LS-mHeps in MC-Dev after a cut or antibody-mediated demyelination, we hypothesised that mHeps exert their effects by modulating factors released by injury. To address this we collected conditioned medium from MC-Inj (CCM; 1 in 4 dilution) and added it to MC-Dev at 16, 19 and 21 DIV, fixing and staining the cultures at 18, 20, 22 and 24 DIV with anti-PLP and the SMI31 antibody. Treatment with CCM resulted in a 33% reduction in myelination compared to control at 24 DIV (Fig. 5A) suggesting the lesion in MC-Inj releases factors which are inhibitory to CNS myelination. This is unlikely to be non-

specific toxicity as neurite density remains unaffected (Fig. 5B). Co-treatment with CCM and LS-mHep6 indicated a trend towards rescue CCM-induced hypomyelination (assessed by the reduction in percentage of myelinated fibres at 24DIV), though this difference did not reach statistical significance ($p = 0.1163$). These data suggest that the LS-mHep6 may modulate the properties of proposed heparin binding factors that are induced by injury (Fig. 5K,L). Representative images are seen in Fig. 5C-J.

Secreted chemokine/cytokine profile is altered after MC-Inj and MC-Demy

As a first step to identifying molecules involved in the effects of mHeps described above, we took a candidate approach, reasoning that chemokines and cytokines which bind heparin/HS could be implicated. To identify specific chemokines and cytokines released in CCM and DCM, we conducted a protein array of conditioned media (see methods for details of array). Fig. 6B-D illustrates the changes in the secreted cytokines standardized to the UCM. Green and red circles indicate only these factors that had a >2 fold increase or <0.8 fold decrease respectively. Several factors were upregulated in both CCM and DCM including CXCL2, CXCL5 and CCL5 (average fold increase of 8.5/16.4, 4.9/6.4 and 3.5/6.6 for CCM and DCM respectively). Striking differences in secreted cytokine profiles were also seen between the two injuries. Many immune associated factors including CCL3, IL-1α, IL-1β, IL-6 and TNF-α were increased in DCM by an average fold change of 9.1, 6.3, 8.9, 3.3 and 4.5 respectively. Interestingly, the same proteins showed no change in CCM, apart from IL-1α and IL-1β, for which a decrease was observed (0.4 and 0.6 respectively). The proteins which were exclusively increased in CCM were trophic factors including HGF, CNTF, Flt-3 ligand and prolactin, which displayed corresponding average fold changes of 3.9, 2.5, 2.6 and 2.2. Comparing the dataset as a whole we observed a significant difference in the proteome profiler between the UCM and the CCM/DCM ($p = 0.0008$ and 0.0004 respectively), suggesting a clear shift in the secretome post-injury. Additionally, there was a significant difference between the CCM and DCM identified in this array ($p = 0.0047$), suggesting some level of injury-type specificity in the CNS injury secretome.

Mass Spectrometry analysis of conditioned medium from MC-Inj and MC-Demy.

As an unbiased approach to identify molecules involved in the effects of mHeps, we used affinity proteomics to explore directly bound proteins that might be mediating the biological responses. To assess which proteins present in the UCM, CCM and DCM interact with LS-mHep7 we performed a protein pull down using an mHep7 affinity column, followed by mass spectroscopy analysis on the eluted samples. Number and distribution of specific and shared proteins can be

seen in the Venn Diagram (Fig 7A). Overall 431 proteins were identified. CCM contained 143 unique proteins; DCM contained 108. 33 proteins were shared between CCM and DCM whereas 47 were specific to UCM. To validate the overall data we performed gene ontology analysis and initially determined the GO enrichment E-value for the entire data set including all three intersections. Heparin binding proteins (GO:0008201) was the highest enriched term with an E value of 5.4 e-15, validating the methodology for pulling down proteins related to heparin binding. Due to the non-quantitative nature, and therefore the inability to make direct comparisons between samples, we carried out TMT LC-MS analysis of the conditioned media.

TMT–LC/MS analysis of conditioned medium from MC-Inj and MC-Demy.

TMT labelling allows the comparison of peptide levels between multiple samples in a single LC-MS run. This multiplexing circumvents problems with reproducibility in serial LC-MS analyses and allows relative quantitation in comparison to control samples. We were able to compare the abundances of LS-mHep7 binding proteins present in each of the CM. Protein levels in the injury CM were standardised to UCM allowing us to state a fold change (FC) after injury. Fig. 7B shows LS-mHep7 binding proteins with a fold change of >1.3 (red) or <0.8 (blue) after injury and a Mascot score of >29 (higher Mascot scores indicate increased confidence in the protein hits). There were 8 mHep7 binding proteins that had elevated abundances after both MC-Inj and MC-Demy represented in the plots by large red symbols (Fig 7B). These include growth hormone releasing hormone receptor which had a massive increase of 327.00 and 136.50 for CCM and DCM respectively (although with a weak Mascot score of 30). Additionally amyloid beta A4 protein (APP) increased 5.7 and 2.0 fold in CCM and DCM (Table 1C). There were 9 proteins which demonstrated an elevated abundance uniquely in the CCM (Table 1A) incuding apolipoprotein D, clusterin, calsyntenin-3 and alpha-2-macroglobulin which showed corresponding fold changes of 2.0, 1.9, 1.8 and 1.6 compared to UCM. There were 23 proteins which demonstrated elevated levels uniquely in the DCM after binding to mHep7 (Table 1B). These proteins are diverse in both structure and function from the large lipid transporter apolipoprotein B-100 (4.57 FC), ECM glycoproteins thrombospondin (4.07 FC) and tenascin C (1.44 FC), protease inhibitor alpha-1-macroglobulin (4.21 FC) and actin binding protein gelsolin (2.35 FC).

A focus on amyloid beta (Aß) 1-42 which is present in the DCM-mHep7 eluate

Amyloid beta A4 protein (APP) is the precursor protein with many cleavage products including the Aß 1-42 peptide and Aß 1-40 peptide. These are the two major C-terminal variants of the Aß protein constituting the majority of Aß peptides and undergo post-secretory aggregation

and deposition in the Alzheimer's disease brain. To investigate the presence of these peptides and validate the TMT-LC/MS analysis an ELISA for the 1-42 peptide and 1-40 peptide was carried out on the eluate from the mHep7 column (Fig 8A,B). This demonstrated that there was a significant increase in concentration for both Aß peptides in the DCM eluate compared to UCM. However, this increase was not observed in the CCM eluate, suggesting that the increased abundance for the APP hit in CCM was due to a different cleavage product. This suggests that the APP cleavage product in the CCM mHep eluate may be from the non amyloidogenic pathway. Moreover, the sequence of peptide fragment identified in the mass spectrometry analysis is a 12 residue peptide corresponding to 439-450 of the precursor protein and represents the soluble product of the initial cleavage by either α-secretase (non-amyloidgenic pathway) or ß-secretase (amyloidgenic pathway); therefore the peptide can be from either pathway.

mHep7 treatment modulates Aß peptide concentration following demyelination

To confirm the exclusive increase of amyloidogenic peptides in MC-Demy, ELISAs were performed on the UCM, CCM and DCM (D0). This demonstrated a sole increase in the DCM of both Aß 1-42 (4 fold) and Aß 1-40 (42 fold) compared to the UCM (Fig 8C-D, $p = 0.0007$ and 0.0017). To establish the effect of mHep treatment on Aß 1-42 and Aß 1-40 concentration, MC-Demy were treated with mHep7 and CM collected at days 1 (D1) and 3 (D3) post treatment. There was a significant increase in Aß 1-42 (1.8 fold) and Aß 1-40 (9 fold) peptides concentration at D1 in the CM following mHep7 treatment compared to the untreated controls (Fig 8E-F, $p = 0.0003$ and 0.001 respectively). However, by D3 there seems to be a significant decrease in Aß 1-42 (0.67 fold) and Aß 1-40 (0.125 fold) peptides concentration compared to the untreated control ($p = 0.0096$ and 0.0001 respectively). The results suggest that treatment with mHep7 can modulate the level of Aß peptides present in the CM.

mHep treatment can overcome Aß (1-42) inhibition of myelination

To examine whether Aß 1-42 peptide has any adverse effect on developmental myelination, an MC-Dev time course was treated with Aß 1-42 peptide (with co-treatment of mHep7). CM was collected and used in a cytotoxicity assay to establish if treatments induced cell death. Treatment of MC-Dev cultures with Aß 1-42 peptide resulted in a 49% reduction in myelination at 24 DIV (Fig 8G-J, $p = 0.0082$). The absence of any effect on neurite density following treatment along with the cytotoxicity assay demonstrated that this was not due to

generic cell death (Fig. 8K). This inhibitory effect could be rescued by co-treatment with mHep7 ($p = 0.032$).

DISCUSSION

Cellular targets for HS: Astrocytes and neurons

Treatment with LS-mHeps showed multiple beneficial outcomes in our MC-Inj cultures by promoting myelination, increasing neurite density and outgrowth and decreasing lesion size. This suggests these compounds are acting on either multiple cellular targets or targeting a specific cell type which in turn can mediate several different cellular processes, such as the astrocyte. After CNS injury astrocytes become reactive and secrete inflammatory molecules that modify the environment around the injury or disease (Williams et al., 2007; Barnett and Linington, 2013; Hara et al., 2017; O'Shea et al., 2017). Moreover, after injury to the adult rat brain there is an overall increase in the quantity of HSPG around the injury site, as well as an increase in mRNA for heparan 2-O-sulphotransferase (HS2ST) and subsequently the level of 2-O-sulphated HS (Properzi et al. 2008). Moreover, changes in sulphation patterns of HSPGs have many effects on axon growth and guidance. For example, HS2ST and heparan 6-O-sulphotransferase (HS6ST) knockout mice have shown multiple navigational errors in their axons, probably due to disturbance of the guidance effects of slit proteins (Pratt et al., 2006), and genetic manipulations of syndecan expression in Drosophila showed similar guidance defects (Johnson et al., 2004).

Our data suggest that the sulphation level or its position on the HS disaccharide is crucial in regulating cellular function. Using our panel of mimetics we found that only the monosulphated forms at the 2-O- and N-sulphated positions promoted neurite outgrowth. This is in agreement with a study that used mutants of the Hst-2 gene thereby reducing 2-O-sulphation on the HS leading to axonal patterning defects (Kinnunen et al. 2004). These experiments suggest that the 2-O-sulphate moiety is involved in neurite outgrowth and pathfinding. However, LS-mHep8 which lacks the 2-O- and 6-O-sulphate also promotes neurite outgrowth, implying that the reduced sulphation level of these mHeps may be contributing to the observed outgrowth. Others have shown that applying HS with different sulphation modifications disrupts axons guidance in the Xenopus visual system, with 2-O- and 6-O-sulphated HS having the most marked effects (Irie et al., 2002). Therefore, it has been postulated that there is a sulphation code that regulates axon guidance (Holt and Dickson, 2005). The LS-mHeps could be directly affecting neurite outgrowth, and astrocytosis through artificially mimicking their interaction with the growing neurite (Lander

et al., 1982), or by indirectly by altering surrounding cellular behavior, creating a permissive environment for outgrowth and re/myelination.

HS role in re/myelination

We originally considered that mHeps might regulate growth factors which act in concert to drive efficient myelination of OPCs. However, there was no effect of their treatment in developmental myelination occurring only when cultures were injured. This could be because endogenous HS are sufficient for developmental myelination but during injury, there are dramatic changes in the extracellular environment suggesting that the LS-mHeps may elicit their effects through interacting with secreted factors present in this aberrant injury environment.

Identification of mHep binding-proteins in CM from MC-Inj and Mc-Demy

To examine the molecular basis for the pro-repair effects in post-injury myelinating cultures we aimed to identify heparin-binding proteins in two ways. Firstly, we examined chemokine/cytokine candidates, and secondly conducted TMT-LC/MS. The chemokine/cytokine array illustrated major differences in the secretome between the MC-Demy and MC-Inj. In the former immune-mediated MC-Demy, inflammatory factors in DCM were more prominent than in CCM. This suggests that these two different culture conditions effect remyelination by distinct mechanisms. For example, IL1α, TNF-α and C1q (found in DCM, see Fig. 6) induce the neurotoxic A1 astrocyte phenotype (Liddelow et al., 2017) suggesting that in MC-Demy this astrocyte phenotype may be affecting remyelination, as previously reported (Nash et al., 2011). Thus, mHeps may be removing or inhibiting, A1 astrocyte inducing factors, therefore promoting remyelination.

Our initial MS analysis was non quantitative but strongly indicated pull down heparin-binding proteins as the most significant group proteins (GO enrichment). GO term analysis (data not shown) confirmed CCM contained many factors involved in neurite outgrowth, guidance migration and changes in astrocyte development. In contrast, DCM contained factors that were related to chemokine signaling and the immune system. Subsequent TMT LC-MS analysis yielded fold changes relative to the uninjured control (UCM), and allowed us to perform direct comparisons between the different CMs with certainty.

The TMT LC-MS data analysis identified a smaller panel of factors but with quantitative data from samples analysed in duplicate. The reduced sensitivity is a likely consequence of the multiplexing approach, but the focus on proteins of a higher abundance may remove outliers and aid in

narrowing our list of candidates. As seen with the cytokine array there was increased expression of immune mediated factors in DCM. The number of proteins present in the CCM was too low to perform GO analysis, but literature searches focussing on secreted factors identified some proteins to have strong correlation with neural cell biology and especially in neuropathology. From this list we selected the following secreted proteins, as they are more likely to be relevant candidates in CNS injury.

Factors found in CCM

Table 1 illustrates candidates isolated from CCM that were expressed at greater than 1.3 fold increase when compared to UCM and less abundant in DCM (less than 1.3 fold increase, and low Mascot score). Apolipoprotein D (ApoD) is a secreted glycoprotein with many roles within lipid transport. It is widely expressed in the developing CNS, and detected in neurons, astrocytes and oligodendrocytes (Ong et al., 1999). ApoD has been associated with neurological disorders (multiple sclerosis, (MS) and Alzheimer's), other inflammatory diseases of the CNS and nerve injury, especially where there is destruction of the myelin sheath (Reindl et al., 2001; Li et al., 2015). Interestingly levels were not above threshold in MC-Demy, suggesting a nerve damage component to its upregulated expression. Thus, ApoD could be sequestered by mHep7 to prevent its negative effects on repair.

A2M, a broad spectrum proteinase inhibitor and a carrier of growth factors was also increased in CCM. A2M has been shown to have neuromodulatory activities by directing the behavior of neurons through sequestering neurotrophic factors (Wolf and Gonias, 1994). Interestingly. A2M has been demonstrated as a marker of neuronal injury and associated with preclinical Alzheimers disease (Varma et al., 2017).

Clusterin (CLU) a small heat shock protein that can act as a molecular chaperone protein was also upregulated. CLU like ApoD, has been implicated in ameliorating oxidative stress in neurodegenerative diseases and may be involved in the death of damaged neurons (Törnqvist et al. 1996). It has been identified in the cerebrospinal fluid (CSF) of patients with MS (van Luijn et al., 2016) and Alzheimers (Wojtas et al., 2007; Matsuoka et al., 2001) and thought to act as a carrier of several proteins across the BBB and CSF barrier including β-amyloid-β (Aβ) (Zlokovic et al., 1996; Ghiso et al., 1993). It has been suggested that CLU directly interacts with Aβ, thereby regulating its clearance from the brain (Bell et al., 2007). Amyloid precursor protein (APP), which was also secreted in CCM and DCM, is known to be upregulated during axonal injury in MS

(Ferguson et al., 1996), and CLU may clear it and thereby prevent aggregation of Aβ. It was also interesting that RAGE was upregulated in the cytokine array as it is thought to play a role in the peripheral re-entry of Aβ into the brain (Deane et al., 2003).

Factors found in DCM

Table 1 shows there were more candidates pulled down in DCM compared to CCM. Several have already been implicated in CNS injury, for example tenascin C (TnC), a glycoprotein synthesized by astrocytes and secreted into the ECM. Increased expression of TnC has been implicated after demyelination *in vivo* (Zhao et al, 2009) and been shown to inhibit OPC differentiation *in vitro* both directly and indirectly through astrocytes (Czopka et al, 2010; Nash et al., 2011). Moreover, knockout of TnC resulted in a favorable outcome on Alzheimer's pathology *in vivo* (Xie et al, 2013). Another ECM glycoprotein Thrombospondin 1 (TSP-1) also appeared to have increased abundance in DCM. TSP-1 interacts with Neuroligin 1 to accelerate synaptogenesis of hippocampal neurons (Xu et al, 2010) but also reported to promote OPC migration (Scott-Drew & ffrench-Constant, 1997).

Another interesting candidate protein in DCM is gelsolin, an actin regulatory factor. Mice lacking gelosin, display a delayed remyelination after PNS crush injuries, presumed due to gelsolin recruiting macrophages to the injury site (Gonçalves et al, 2010). Moreover, gelsolin knock-out had wrapping defects in the CNS, (Zuchero et al, 2015). This implies gelsolin might have a dual role after injury, firstly through the recruitment of immune cells to clear debris and secondly facilitating oligodendrocyte axon ensheathment.

Candidate factors identified in both DCM and CCM

In Table 1 it can be seen that a few candidates were upregulated in both CCM and DCM and therefore may relate to promoting myelination. One candidate, growth hormone releasing hormone receptor has been detected in the CNS, and its ligand activity promotes the secretion of insulin-like growth factor (IGF-1, Zhao et al., 2008), a known mitogen for OPCs and an important regulator of brain development, maintenance and neurogenesis (Aberg, 2010). It is possible that mHep7 sequesters IGF-1 and allows the OPCs to differentiate into mature oligodendrocytes. Moreover, APP was identified in both CMs. HS has been shown to interact with Aβ peptides and thus been implicated in facilitating Aβ cytotoxicity and accelerating amyloid fibril formation (Sandwall et al, 2010; Castillo et al, 1997). Additionally, infusion with Aβ and HS into rat brains resulted in increased amyloidosis compared to Aβ alone (Snow et al, 1994). This suggests that

endogenous HS somewhat aids Aβ aggregation pathology. Aβ has been shown to be secreted in excess following traumatic injury (Gentleman et al., 1993) and MS lesions (Panjoohesh-Gani et al., 2014). Although not understood in these pathological conditions Aβ has been reported to have negative correlation with functional outcome and induce microglia activation, inflammation and neuronal cell death (Matsuoka et al., 2001).

Due to the detection of Aβ in MC-Inj and MC-Demy and its known role in CNS pathology we decided to focus more on its function and interaction with mHeps in these cultures. Since APP has numerous different fragment peptides it was important to determine the peptides identified in the TMT/LC-MS. ELISAs of the mHep7 eluates and CMs suggests that after demyelination in MC-Demy Aβ peptides (1-40/42) are secreted, and that the degradation of these peptides is modulated directly by mHep treatment. Previously, it has been demonstrated that treatment with Aβ 1-42 inhibits OPC differentiation (Horiuchi et al, 2010), in this study we developed this further showing that the effect was present at the level of myelination and could be rescued through mHep co-treatment. However it appears that the APP detected in but with quantitative data from samples analysed in duplicate the CCM mHep7 eluate mass spec analysis was not Aβ 1-40 or 1-42 peptides, suggesting it was the P3 peptide from the non-amyloidgenic pathway. This peptide is the equivalent of Aβ 17-40/42, although this fragment does not assemble into soluble oligomers, it does possess cellular toxic properties (Dulin et al, 2008; Wei et al, 2002). Hence the P3 peptide could be a mHep7 modulated negative injury factor secreted after MC-Inj. As Aβ peptides have been reported in both neurodegeneration and traumatic injury, they could be a valuable target for mHep7 and the action of sequestering or inhibiting aggregation, could promote neurite outgrowth and myelination in MC-Inj and MC-Demy. Recent studies are already looking at modified heparins and Alzheimer's, but at the role of modified heparins regulating Alzheimer's-related enzymes, specifically, BACE1 (Scholefield et al, 2003).

In summary, the present study has demonstrated beneficial effects of LS-mHeps on repair in models of CNS damage specifically promoting neurite outgrowth and myelination by modifying the properties of secreted factors generated after injury. Our data has identified multiple protein candidates for mediating these effects and thus plausible underlying mechanisms. Moreover, this illustrates the complexity of mediating repair and highlights that therapeutics need to target many factors, as seen by LS-mHeps. Furthermore, we show Aβ peptides can play a role in demyelination. Finally, based on the protein hits and the relation of some of these proteins to other neurological

disease such as AD, these novel compounds could also have therapeutic potential in other neurological disorders.

LEGENDS

Table 1. TMT-LC/MS identified candidates.

List of complete candidates that were identified with Mascot scores greater than 30 and fold increase greater than 1.3 in A) both CCM and DCM, B) CCM only and C) DCM only. Candidates that are secreted and of interest in these cultures are highlighted in bold and reflect those indicated in Fig. 7B.

Figure 1. LS-mHep promote myelination and neurite outgrowth.

Representative images of MC-Inj of a control cut (A) and after treatment with the LS-mHep6-8 showing a promotion of myelination adjacent to the lesion following a single treatment (C-E). In contrast the HS-mHep1 showed a non-significant decrease the levels of myelination (B). Quantification of the images are shown in F ($p = 0.017$, $p < 0.0001$ and $p = 0.0001$ for mHep6, 7 and 8 respectively). Only mHep6 significantly promoted neurite density adjacent to the lesion when compared to control cultures ($p = 0.0127$) (G). Representative images of the lesion after cutting with a scalpel blade in MC-Inj (H), and after HS-mHep1 treatment showing no effect on neurite outgrowth (I). Significant neurite outgrowth across the lesion was seen after treatment with LS-mHep6-8 compared to control untreated cultures ($p = 0.0172$, $p < 0.0001$ and $p = 0.0029$ for mHep6, 7 and 8 respectively) (J-M). Representative image of lesion size is shown in (H-L) identified by dashed line. An increase is lesion width following treatment with HS-mHep1 (564.5 μm) was seen, when compared to a control lesion (400 μm $p = 0.0026$). LS-mHep6-8 had no effect on lesion width (N). Statistical test used was one-way ANOVA with post-hoc Dunnett's multi-comparison correction, n = 6 and error bars SEM, scale bar, 25 μm. SMI31-red, PLP-green.

Figure 2. LS-mHeps do not effect OPC proliferation but promote the number of OL adjacent to the lesion and process extension on nanofibers.

A-C) mHep treatment had no effect on the proliferation of OPCs. A,B are representative images of control and PDGF/FGF treated OPCs respectively, scale bars-100 μm. Quantification of proliferation was determined by percentage of EdU positive cells which demonstrated no difference between control and mHep treated OPCs (C), error bars- SEM. D-F) LS-mHep6 and 7 treatment caused an increase in the number of OLs adjacent to the lesion ($p = 0.0133$ and $p = 0.0002$ respectively). D) Microscope image stained for PLP (green) and SMI-31 (red) at lesion

edge of MC-Inj. E) Same image quantified for PLP-IR (OL) after LS-mHep treatment. In contrast, HS-mHep1 treated cultures showed a significant decrease in the number of OLs compared to control cultures ($p = 0.00336$). Representative images of OPCs plated on nanofibres in the presence of DMEM-BS (G), HS-mHep1 (H), LS-mHep6 (I) and LS-mHep7 (J). K) Quantification of cell area demonstrated that LS-mHep7 treatment resulted in increase in the OL cell size, compared to the untreated control ($p < 0.0001$). L) Quantification of myelin sheath length demonstrated that LS-mHep6 and 8 treatments statistically promoted sheath length compared to controls ($p = 0.0001$ for both). As expected GF treated OPCs had a reduced OL cell size ($p = 0.0005$) with limited process extension along the nanofibers (K, L). Statistical test used was one-way ANOVA with post-hoc Dunnett's multi-comparison correction, n=4 and scale bars, 25 μm and 50 μm, error bar-SEM, PLP-green, SMI31-red.

Figure 3. 2-*O*-sulphated mHeps had no effect on the development of myelination but mHep1 and the *N*-sulphated isoform affected myelinated fibres.

A-D) Representative images of MC-Dev control or mHep (1 ng/ml added at 13 and 20 DIV) treated cultures showing myelinated fibres, SMI31-red and PLP-green (scale bars-100μm).

E) Quantification of myelination relative to the untreated control showing no significant difference in myelination levels after mHep treatment. F) Neurite density was also unaltered by mHep treatment. Error bars-SEM (N=3). G-J) Representative images of MC-Dev control or mHep (1 ng/ml added at 24 DIV) treated cultures. Quantification of myelination (K) demonstrated a reduction in myelination levels post HS-mHep1 ($p = 0.0033$) and LS-mHep7 ($p = 0.0163$) treatments on the mature cultures. While neurite density remained unchanged (L). Scale bars-25 μm, error bar-SEM (n=4).

Figure 4. LS-mHeps have significant effects on remyelination in MC-Demy.

Myelinating cultures were allowed to mature until 24 DIV at which point they were demyelinated via overnight incubation with the anti-MOG specific antibody Z2 (100 ng/ml) and rabbit complement (100 μg/ml). Treatment occurred at 25 DIV (1 ng/ml) and then cultures were allowed to recover till 30 DIV, at which point they were immunolabelled with SMI31 (red, neurites) and AA3 (green, myelin). A-F) Representative images of MC-Demy treated with anti-MOG and complement on 25 DIV (B) and 30 DIV (C) and treated with the mHeps (D-F) (scale bars-100μm).

G) Quantification of myelination showing treatment with mHeps resulted in an 87%, 71% and 81% increase in remyelination compared to the demyelinated control (Demy5) for LS-mHeps6, 7

and 8 respectively (one way ANOVA with Holm-Sidak multiple comparison, p = 0.0002, 0.0004 and 0.0002), error bars SEM. H). Quantification of neurite density showed no change in density with treatment implying no adverse toxic effects on the cultures.

Figure 5. Cut conditioned medium (CCM) significantly reduces developmental myelination, which is partially overcome by LS-mHeps.

CCM was collected from MC-Inj at 25 DIV and used to treat MC-Dev cultures at 16, 19 and 21 DIV (1 in 4 dilution). C-J) Representative images of control and CCM treated cultures, immunolabelled with SMI31-red and PLP-green. Scale bar 100 μm. A,B) Quantification of myelination and neurite outgrowth over time after CCM treatment showing no difference in the development of myelination between CCM treated and control cultures at 18, 20 and 22 DIV. However, at 24 DIV there was a significant 33% reduction in myelination of the CCM treated cultures compared to the control (p = 0.0031). K,L) Quantification of myelination and neurite density of MC-Demy after a combined treatment of CCM and LS-mHep6 showed an increase in percentage of myelinated fibres so as to be non-statistically different from the untreated control. Quantification of neurite density after treatment with CCM showed no adverse effects on neurites (One way ANOVA with Dunnett multiple comparison), scale bars 100 μm (n = 3).

Figure 6. Differences in chemokine/cytokine secretion profile after CNS injury.

Cut conditioned media (CCM), demyelinated conditioned medium (DCM) and control conditioned medium (UCM) were collected from MC-Inj, MC-Demy and MC-Dev respectively on 25 DIV and the cytokine profile assessed using a rat cytokine array. A) The dots blots of the cytokine arrays for each of the conditioned media. B-C) Tables illustrating the fold changes with (+/- SD) of expression changes in both CCM/DCM (B) CCM (C) and DCM (D) compared to UCM, the green and red spheres indicate >2 fold increase and <0.8 fold decrease respectively (n=3).

Figure 7. Modified heparin 7 pull down experiment of CM from MC-Inj (CCM) and MC-Demy (DCM).

Condition media collected from control cultures (UCM), MC-Inj (CCM) and MC-Demy (DCM), was run through a mHep7 column, to select mHep7 binding proteins and identify potential candidates (5 ml CM used per each pull down, CM a combination of at least n=5). A) Venn diagram depicting the number of candidates both unique to and shared by each CM. It can be seen that the number of candidates obtained decreased as methods were modified from a non-

quantitative LC/MS to TMT-LC/MS. B) Graph generated using R package UpsetR, a matrix-based layout showing the intersections of all three CM data sets. Large symbols indicate the fold increase in shared candidates in DCM and CCM while small red symbols are candidates increased when compared to control and blue symbols are candidates decreased when compared to control. Circles represent secreted candidates, with triangles depicting intracellular candidates and squares for candidates that have no reports in the literature A-H are interesting candidates based on literature searches identified for discussion.

Figure 8. Validation of amyloid beta as a candidate for demyelination. A-B) ELISAs of the mHep7 eluate. Concentration of Aß 1-42 ($p = 0.0007$) and Aß 1-40 ($p = 0.0017$) is significantly increased in the DCM mHep7-eluate compared to the UCM mHep7eluate. C-D) ELISAs of CM after injury (Day 0). There was a large increase in the level of Aß 1-42 and Aß 1-40 peptide secretion immediately after demyelination (D0) compared to the uninjured control (both $p < 0.0001$). E-F) MC-Demy cultures were treated with mHep7 following demyelination. CM was collected at 26 and 28 DIV (corresponding to days 1 and 3 post treatment). E) Graph shows a statistically significant increase in Aß 1-42 present in DCM 24 hours after mHep7 treatment (D1) compared to untreated control ($p = 0.0003$). However by day 3 post treatment (D3) there was a significant reduction in Aß 1-42 present in the CM following mHep7 treatment ($p = 0.0096$). The same pattern was observed with Aß 1-40 with treatment leading to an increase in concentration shortly after treatment at D1 ($p = 0.0010$), but by D3 there seems to be a significant decrease in the level of Aß 1-40 following mHep treatment compared to untreated control ($p = 0.0001$). G-K) Cultures were treated at 16, 19 and 21 DIV at 1 μM (co-treatments with mHep7 at 100 ng/mL). G-I) Representative images of control, Aß treated and Aß + mHep7 treated cultures at 24 DIV, immunolabelled with SMI31-red and PLP-green (Scale bar, 100 μm). J) Quantification of myelination over time showing a significant decrease in developmental myelination at 24 DIV after Aß treatment ($p = 0.0082$) this is overcome by mHep7 co-treatment ($p = 0.0321$). Quantification of neurite density over time suggests no effect of either treatment on neurite density (data not shown). K) LDH release cytotoxity assay demonstrating no statistically significant effect on cell death at 24 DIV following Aß treatment or mHep7 co-treatment.

References

Aberg, D. (2010). Role of the growth hormone/insulin-like growth factor 1 axis in neurogenesis. *Endocr Dev, 17*, 63-76. doi: 10.1159/000262529.

Akpunarlieva, S. Weidt, S., Lamasudin, D., Naula, C., Henderson, D., Barrett, M., Burgess, K., Burchmore, R. (2017). Integration of proteomics and metabolomics to elucidate metabolic adaptation in Leishmania. *J Proteomics, 155*, 85-98. doi: 10.1016/j.jprot.2016.12.009.

Alexa, A., & Rahnenfuhrer, J. (2016). topGO: Enrichment Analysis for Gene Ontology. R package version 2.24.0.

Barnett, S. C., & Linington, C. (2013). Myelination do astrocytes play a role? *Neuroscientist 19*, 442-450. doi: 10.1177/1073858412465655.

Bell, R.D., Sagare, A. P., Friedman, A. E., Bedi, G.S., Holtzman, D. M., Deane, R., Zlokovic, B. V. (2007) Transport pathways for clearance of human Alzheimer's amyloid beta-peptide and apolipoproteins E and J in the mouse central nervous system. J Cereb Blood Flow Metab 27:909–918

Bilić, P., Guillemin, N., Kovačević, A., Beer Ljubić, B., Jović, I., Galan, A., Eckersall, P. D., Burchmore, R., Mrljak, V. (2018). Serum proteome profiling in canine idiopathic dilated cardiomyopathy using TMT-based quantitative proteomics approach. *J Proteomics. 179,* 110-121. doi: 10.1016/j.jprot.2018.03.007.

Bishop, R. J., Schuksz, M., Esko, J. D. (2007). Heparan sulpate proteoglycans fine-tune mammalian physiology. *Nature, 446,* 1030-1037.

Boomkamp, S. D., Riehle, M. O., Wood, J., Olson, M. F., Barnett, S. C. (2012). The development of a rat in vitro model of spinal cord injury demonstrating the additive effects of Rho and ROCK inhibitors on neurite outgrowth and myelination. *Glia, 60,* 441-456. doi: 10.1002/glia.22278.

Boomkamp, S. D., McGrath, M. A., Houslay, M. D., Barnett, S. C. (2014). Epac and the high affinity rolipram binding conformer of PDE4 modulate neurite outgrowth and myelination using an in vitro spinal cord injury model. *Br J Pharmacol, 171,* 2385-2398. doi: 10.1111/bph.12588.

Bottenstein, J. E., & Sato, G. H. (1979). Growth of rat neuroblastoma cell line in serum-free supplemented medium. *Proc Natl Acad Sci, 76.* 514-317.

Carpenter, A. E., Jones, T. R., Lamprecht, M. R., Clarke, C., Kang, I. H., Friman, O., Guertin, D, A., Chang, J, H., Lindquist, R, A., Moffat, J., Golland, P., Sabatini, D. M,. (2006). CellProfiler: image analysis software for identifying and quantifying cell phenotypes. *Genome Biol 7*, R100. doi: 10.1186/gb-2006-7-10-r100

Castillo, G. M., Ngo, C., Cummings, J., Wight, T. N., Snow, A. D. (1997). Perlecan binds to the beta-amyloid proteins (A beta) of Alzheimer's disease, accelerates A beta fibril formation, and maintains A beta fibril stability. *J Neurochem 69*, 2452-2465.

Changyaleket, B., Deliu, Z., Chignalia, A. Z., Feinstein, D. (2017). Heparanase: potential roles in multiple sclerosis. *J Neuroimmunol 210,* 72-81. doi: 10.1016/j.jneuroim.2017.07.001.

Cui, H., Freeman, C., Jacobson, G. A., Small, D. H. (2013). Proteoglycans in the central nervous system: Role in development. Neural repair and Alzheimers disease. *IUMB Life, 65,* 108-120. doi: 10.1002/iub.1118.

Czopka, T., von Holst, A., ffrench-Constant, C., Faissner, A. (2010). Regulatory mechanisms that mediate tenascin C-dependent inhibition of oligodendrocyte precursor differentiation. *J Neurosci, 30,* 12310-123122. doi: 10.1523/JNEUROSCI.4957-09.2010.

Deane, R., Du Yan, S., Submamaryan, R, K., LaRue, B., Jovanovic, S., Hogg, E., Welch, D., Manness, L., Lin, C., Yu, J., Zhu, H., Ghiso, J., Frangione, B., Stern, A., Schmidt, A. M., Armstrong, D. L., Arnold, B., Liliensiek, B., Nawroth, P., Hofman, F., Kindy, M., Stern, D,, Zlokovic, B. (2003). RAGE mediates amyloid-beta peptide transport across the blood-brain barrier and accumulation in brain. *Nat Med, 9,* 907-913.

Dulin, F., Léveillé, F., Ortega, J. B., Mornon, J. P., Buisson, A., Callebaut, I., Colloc'h, N. (2008). P3 peptide, a truncated form of A beta devoid of synaptotoxic effect, does not assemble into soluble oligomers. *FEBS Lett, 582,* 1865-1870. doi: 10.1016/j.febslet.2008.05.002.

Dumont, R. J., Okonkwo, D. O., Verma, S., Hurlbert, R. J., Boulos, P. T., Ellegala, D. B., Dumont, A. S. (2001). Acute spinal cord injury, part I: pathophysiologic mechanisms. *Clin Neuropharmacol, 24,* 254-264.

Elliott, C., Lindner, M., Arthur, A., Brennan, K., Jarius, S., Hussey, J., Chan, A., Stroet, A., Olsson, T., Willison, H. J., Barnett, S. C., Meinl, E., Linington, C. (2012). Functional identification of pathogenic autoantibody responses in patients with multiple sclerosis. *Brain, 135,* 1819-1833. doi: 10.1093/brain/aws105.

Fairless, R., Frame, M. C., Barnett, S. C. (2005). N-cadherin differentially determines Schwann cell and olfactory ensheathing cell adhesion and migration upon contact with astrocytes. Molecular Cell Neurosci, 8, 253-263. doi: 10.1016/j.mcn.2004.09.009

Ferguson, B., Matyszak, M. K., Esiri, M. M., Perry, V. H. (1997). Axonal damage in acute multiple sclerosis lesions. *Brain, 120,* 393-399.

Filous, A. R., & Silver, J. (2016). Targeting astrocytes in CNS injury and disease: A translational research approach. *Prog Neurobiol, 144,* 173-187. doi: 10.1016/j.pneurobio.2016.03.009

Gentleman, S. M., Nash, M. J., Sweeting, C. J., Graham, D. I., Roberts, G, W. (1993). Beta-amyloid precursor protein (beta APP) as a marker for axonal injury after head injury. *Neurosci Lett, 160,* 139-144.

Ghiso, J. Matsubara, E. Koudinov, A., Choi-Miura, N. H., Tomita, M., Wisniewski, T., Frangione, B. (1993). The cerebrospinal-fluid soluble form of Alzheimer's amyloid beta is complexed to SP-40,40 (apolipoprotein J), an inhibitor of the complement membrane-attack complex. *Biochem J, 293*, 27-30.

Gonçalves, A. F., Dias, N. G., Moransard, M., Correia, R., Pereira, J. A., Witke, W., Suter, U., Relvas, J. B. (2010). Gelsolin is required for macrophage recruitment during remyelination of the peripheral nervous system. *Glia, 58,* 706-715. doi: 10.1002/glia.20956.

Hara, M., Kobayakawa, K., Ohkawa, Y., Kumamaru, H., Yokota, K., Saito, T., Kijima, K., Yoshizaki, S., Harimaya, K., Nakashima, Y., Okada, S. (2017). Interaction of reactive astrocytes with type I collagen induces astrocytic scar formation through the integrin-N-cadherin pathway after spinal cord injury. *Nat Med, 23*, 818-828. doi: 10.1038/nm.4354.

Higginson, J. R., Thompson, S. M., Santos-Silva, A., Guimond, S. E., Turnbull, J. E., Barnett, S. C. (2012). Differential sulphation remodelling of heparan sulphate by extracellular 6-O-sulphatases regulates fibroblast growth factor-induced boundary formation by glial cells. *J Neurosci, 32*, 15902-15912. doi: 10.1523/JNEUROSCI.6340-11.2012.

Holt, C. E., & Dickson, B. J. (2005). Sugar codes for axons? *Neuron, 46,* 169-172. doi: 10.1016/j.neuron.2005.03.021

Horiuchi, M., Maezawa, I., Itoh, A., Wakayama, K., Jin, L. W., Itoh, T., Decarli, C. (2012). Amyloid β1-42 oligomer inhibits myelin sheet formation in vitro. *Neurobiol Aging, 33*, 499-509. doi: 10.1016/j.neurobiolaging.2010.05.007.

Irie, A., Yates, E. A., Turnbull, J. E., Holt, C. E. (2002). Specific heparan sulphate structures involved in retinal axon targeting. *Development, 129,* 61-70.

Johnson, K. G., Ghose, A., Epstein, E., Lincecum, J., O'Connor, M . B., Van, V. D. (2004) Axonal heparan sulphate proteoglycans regulate the distribution and efficiency of the repellent slit during midline axon guidance. Curr Biol, 14, 499-504. doi: 10.1016/j.cub.2004.02.005

Kinnunen, T., Townsend, J., Turnbull, J. (2004). Heparan sulphate is essential for neuron migration and axon outgrowth in Caenorhabditis elegans. Int J Exp Pathol, 85, A69-A70.

Lakatos, A., Franklin, R. J. M., Barnett, S. C. (2000). Olfactory ensheathing cells and Schwann cells differ in their in vitro interactions with astrocytes. Glia, 32, 214-225.

Lander, A. D., Fujii, D. K., Gospodarowicz, D., Reichardt, L. F. (1982). Characterization of a factor that promotes neurite outgrowth: evidence linking activity to a heparan sulphate proteoglycan. *J Cell Biol, 94*, 574-685.

Lee, S., Leach, M. K., Redmond, S. A., Chong, S.Y., Mellon, S. H., Tuck, S. J., Feng, Z. Q., Corey, J. M., Chan, J. R. (2012). A culture system to study oligodendrocyte myelination processes using engineered nanofibers. *Nat Methods, 9,* 917-922. doi: 10.1038/nmeth.2105

Li, H., Ruberu, K., Muñoz, S. S., Jenner, A. M., Spiro, A., Zhao, H., Rassart, E., Sanchez, D., Ganfornina, M. D., Karl, T., Garner, B. (2015). Apolipoprotein D modulates amyloid pathology in APP/PS1 Alzheimer's disease mice. *Neurobiol Aging, 36,* 1820-1833. doi: 10.1016/j.neurobiolaging.2015.02.010

Liddelow, S. A., Guttenplan, K. A., Clarke, L. E., Bennett, F. C., Bohlen, C. J., Schirmer, L., Bennett, M. L., Münch, A. E., Chung, W. S., Peterson, T. C., Wilton, D. K., Frouin, A., Napier, B. A., Panicker, N., Kumar, M., Buckwalter, M. S., Rowitch, D. H., Dawson, V. L., Dawson, T.M., Stevens, B., Barres, B.A. (2017). Neurotoxic reactive astrocytes are induced by activated microglia. *Nature, 541*, 481-487. doi: 10.1038/nature21029.

Lindner, M., Thümmler, K., Arthur, A., Brunner, S., Elliott, C., McElroy, D., Mohan, H., Williams, A., Edgar, J. M., Schuh, C., Stadelmann, C., Barnett, S. C., Lassmann, H., Mücklisch, S., Mudaliar, M., Schaeren-Wiemers, N., Meinl, E., Linington, C. (2015). Fibroblast growth factor signalling in multiple sclerosis: inhibition of myelination and induction of pro-inflammatory environment by FGF9. *Brain, 138*, 1875-1893. doi: 10.1093/brain/awv102

Matsuoka, Y., Picciano, M., Malester, B., LaFrancois, J., Zehr, C., Daeschner, J. M., Olschowka, J. A., Fonseca, M. I., O'Banion, M. K., Tenner, A. J., Lemere, C. A., Duff, K. (2001). Inflammatory responses to amyloidosis in a transgenic mouse model of Alzheimer's disease. *Am J Pathol, 158*, 1345-1354. doi: 10.1016/S0002-9440(10)64085-0

Miron, V. E., Boyd, A., Zhao, J. W., Yuen, T. J., Ruckh, J. M., Shadrach, J. L., van Wijngaarden, P., Wagers, A. J., Williams, A., Franklin, R J., Ffrench-Constant C. (2013). M2 microglia and macrophages drive oligodendrocyte differentiation during CNS remyelination. Nat Neurosci, 16, 211–1218. doi: 10.1038/nn.3469.

Nash, B., Thomson, C. E., Linington, C., Arthur, A. T., McClure, J. D., McBride, M. W., Barnett, S. C. (2011). Functional duality of astrocytes in myelination. *J Neurosci, 31*, 13028-13038. doi: 10.1523/JNEUROSCI.1449-11.2011.

Noble, M., & Murray, K. (1984). Purified astrocytes promote the in vitro division of a bipotential glial progenitor cell. EMBO J, 3, 2243–2247.

O'Neill, P., Lindsay, S. L., Damianou, A., Guimond, S. E., Fagoe, N., Verhaagen, J., Turnbull, J. E., Riddell, J. S., Barnett, S. C. (2017). Sulphatase mediated manipulation of the astrocyte-Schwann cell interface. *Glia, 65,* 19-33. doi: 10.1002/glia.23047.

Ong, W. Y., Lau, C. P., Leong, S. K., Kumar, U., Suresh, S., Patel, S. C. (1999). Apolipoprotein D gene expression in the rat brain and light and electron microscopic immunocytochemistry of apolipoprotein D expression in the cerebellum of neonatal, immature and adult rats. *Neuroscience, 90,* 913-922.

O'Shea, T. M., Burda, J. E., Sofroniew, M. V. (2017). Cell biology of spinal cord injury and repair. J Clin Invest, 127, 3259-3270. doi: 10.1172/JCI90608

Pajoohesh-Ganji, A., Burns, M. P., Pal-Ghosh, S., Tadvalkar, G., Hokenbury, N. G., Stepp, M. A., Faden, A. I. (2104). Inhibition of amyloid precursor protein secretases reduces recovery after spinal cord injury. Brain Res, 1560, 73-82. doi: 10.1016/j.brainres.2014.02.049.

Pratt, T., Conway, C. D., Tian, N. M., Price, D. J., Mason, J. O. (2006). Heparan sulphation patterns generated by specific heparan sulphotransferase enzymes direct distinct aspects of retinal axon guidance at the optic chiasm. *J Neurosci, 26,* 6911-6923. doi: 10.1523/JNEUROSCI.0505-06.2006

Properzi, F., Lin, R., Kwok, J., Naidu, M., van Kuppevelt, T. H., Ten Dam, G. B., Camargo, L. M., Raha-Chowdhury, R., Furukawa, Y., Mikami, T., Sugahara, K., Fawcett, J. W. (2008). Heparan sulphate proteoglycans in glia and in the normal and injured CNS: expression of sulphotransferases and changes in sulphation. Eur J Neurosci, 27, 593-604. oi: 10.1111/j.1460-9568.2008.06042.x.

Reindl, M., Knipping, G., Wicher, I., Dilitz, E., Egg, R., Deisenhammer, F., Berger, T. (2001). Increased intrathecal production of apolipoprotein D in multiple sclerosis. *J Neuroimmunol, 119*, 327-32.

Reynolds, B. A., & Weiss, S. (1996). Clonal and population analyses demonstrate that an EGF-responsive mammalian embryonic CNS precursor is a stem cell. *Dev Biol, 175,* 1-13. doi: 10.1006/dbio.1996.0090

Santos-Silva, A., Fairless, R., Frame, M., Montague, P., Smith, G. M., Toft, A., Riddell, J. S., Barnett, S. C. (2007). OECs lack a heparin te proteoglycan that Schwann cells use to induce the astrocyte stress response mediated via FGFR1 activation. *J Neurosci, 27,* 7154-7167. doi: 10.1523/JNEUROSCI.1184-07.2007

Sandwall, E., O'Callaghan, P., Zhang, X., Lindahl, U., Lannfelt, L., Li, J. P. (2010). Heparan sulphate mediates amyloid-beta internalization and cytotoxicity. Glycobiology, 20, 533-41. doi: 10.1093/glycob/cwp205

Scholefield, Z., Yates, E. A., Wayne, G ., Amour, A., McDowell, W., Turnbull, J. E. (2003). Heparan sulphate regulates amyloid precursor protein processing by BACE1, the Alzheimer's beta-secretase. J Cell Biol163:97-107. Doi: 10.1083/jcb.200303059

Scott-Drew, S., & ffrench-Constant, C. (1997). Expression and function of thrombospondin-1 in myelinating glial cells of the central nervous system. J Neurosci Res, 50, 202-214. doi: 10.1002/(SICI)1097-4547(19971015)50:2<202::AID-JNR9>3.0.CO;2-J

Snow, A. D., Sekiguchi, R. T., Nochlin, D., Kalaria, R. N., Kimata, K. (1994). Heparan sulphate proteoglycan in diffuse plaques of hippocampus but not of cerebellum in Alzheimer's disease brain. *Am J Pathol, 144,* 337-347.

Sorensen, A., Moffat, K., Thomson, C., Barnett, S. C. (2008). Astrocytes, but not olfactory ensheathing cells or Schwann cells, promote myelination of CNS axons in vitro. Glia, 56, 750-763. doi: 10.1002/glia.20650

Sommer, I., & Schachner, M. (1981). Monoclonal antibodies (O1 to O4) to oligodendrocyte cell surfaces: an immunocytological study in the central nervous system. Dev Biol, 83, 311-327.

Thomson, C. E., McCulloch, M., Sorenson, A., Barnett, S. C., Seed, B. V., Griffiths, I. R., McLaughlin, M. (2008). Myelinated, synapsing cultures of murine spinal cord--validation as an in vitro model of the central nervous system. *Eur J Neurosci, 28,* 1518-1535. doi: 10.1111/j.1460-9568.2008.06415.x.

Törnqvist, E., Liu, L., Aldskogius, H., Holst, H. V., Svensson, M. (1996). Complement and clusterin in the injured nervous system. Neurobiol Aging, 17, 695-705.

van Luijn, M. M., van Meurs, M., Stoop, M. P., Verbraak, E., Wierenga-Wolf, A. F., Melief, M. J., Kreft, K. L., Verdijk, R. M., 't Hart, B. A., Luider, T. M., Laman, J. D., Hintzen, R.Q. (2016). Elevated Expression of the Cerebrospinal Fluid Disease Markers Chromogranin A and Clusterin in Astrocytes of Multiple Sclerosis White Matter Lesions. *J Neuropathol Exp Neurol, 75,* 86-98. doi: 10.1093/jnen/nlv004

Varma, V.R., Varma, S., An, Y., Hohman, T. J., Seddighi, S., Casanova, R., Beri, A., Dammer, E. B., Seyfried, N. T., Pletnikova, O., Moghekar, A., Wilson, M. R., Lah, J. J., O'Brien, R. J., Levey, A. I., Troncoso, J. C., Albert, M. S., Thambisetty, M. (2017). Alpha-2 macroglobulin in Alzheimer's disease: a marker of neuronal injury through the RCAN1 pathway. *Mol Psychiatry 22,* 13-23. doi: 10.1038/mp.2016.206.

Wei, W., Norton, D. D., Wang, X., Kusiak, J. W. (2002). Abeta 17-42 in Alzheimer's disease activates JNK and caspase-8 leading to neuronal apoptosis. Brain, 125, 2036-2043.

Wilby, M. J., Muir, E. M., Fok-Seang, J., Gour, B. J., Blaschuk, O. W., Fawcett, J. W. (1999). N-Cadherin inhibits Schwann cell migration on astrocytes. *Mol Cell Neurosci, 14*, 66-84. doi: 10.1006/mcne.1999.0766

Williams, A., Piaton, G., Lubetzki, C. (2007). Astrocytes--friends or foes in multiple sclerosis? *Glia, 55,* 1300-1312. doi: 10.1002/glia.20546

Wiśniewski, J. R., Zougman, A., Nagaraj, N., Mann, M. (2009). Universal sample preparation method for proteome analysis. *Nat Methods, 6*, 359-362. doi: 10.1038/nmeth.1322

Wojtas, A. M., Kang, S. S., Olley, B. M., Gatherer, M., Shinohara, M., Lozano, P. A., Liu, C. C., Kurti, A., Baker, K. E., Dickson, D. W., Yue, M., Petrucelli, L., Bu, G., Carare, R. O., Fryer, J. D. (2017). Loss of clusterin shifts amyloid deposition to the cerebrovasculature via disruption of perivascular drainage pathways. *Proc Natl Acad Sci, 114,* E6962-E6971. doi: 10.1073/pnas.1701137114

Wolf, B. B., & Gonias, S. L. (1994). Neurotrophin binding to human alpha 2-macroglobulin under apparent equilibrium conditions. *Biochem, 33,* 11270-11277.

Xie, K., Liu, Y., Hao, W., Walter, S., Penke, B., Hartmann, T., Schachner, M., Fassbender, K. (2013). Tenascin-C deficiency ameliorates Alzheimer's disease-related pathology in mice. *Neurobiol Aging, 34,* 2389-2398. doi: 10.1016/j.neurobiolaging.2013.04.013.

Xu J, Xiao N, Xia J (2010) Thrombospondin 1 accelerates synaptogenesis in hippocampal neurons through neuroligin 1. Nat Neurosci 13:22-24.

Yamamura, T. Konola, J. T., Wekerle, H., Lees, M. B. (1991). Monoclonal antibodies against myelin proteolipid protein: identification and characterization of two major determinants. J *Neurochem, 57,* 1671-1680.

Zuchero, J.B., Fu, M. M., Sloan, S. A., Ibrahim, A., Olson, A., Zaremba, A ., Dugas, J. C., Wienbar, S., Caprariello, A. V., Kantor, C., Leonoudakis, D., Lariosa-Willingham, K., Kronenberg, G., Gertz, K., Soderling, S. H., Miller, R. H., Barres, B. A. (2015). CNS myelin wrapping is driven by actin disassembly. *Dev Cell, 34*, 152-167. doi: 10.1016/j.devcel.2015.06.011.

Zhao, L., Yano, T., Osuga, Y., Nakagawa, S., Oishi, H., Wada-Hiraike, O., Tang, X., Yano, N., Kugu, K., Schally, A. V., Taketani, Y. (2008). Cellular mechanisms of growth inhibition of human endometrial cancer cell line by an antagonist of growth hormone-releasing hormone. *Int J Oncol, 32,* 593-601.

Zhao, C., Fancy, S. P., Franklin, R. J., ffrench-Constant, C. (2009). Up-regulation of oligodendrocyte precursor cell alphaV integrin and its extracellular ligands during central nervous system remyelination. *J Neurosci Res, 87,* 3447-3455. doi: 10.1002/jnr.22231.

Zlokovic, B. V., Martel, C. L., Matsubara, E., McComb, J. G., Zheng, G., McCluskey, R. T., Frangione, B., Ghiso, J. (1996). Glycoprotein 330/megalin: Probable role in receptor-mediated transport of apolipoprotein J alone and in a complex with Alzheimer disease amyloid beta at the blood-brain and blood-cerebrospinal fluid barriers. Proc Natl Acad Sci, 93, 4229-4334.